

# Histone Chaperone Paralogs Have Redundant, Cooperative, and Divergent Functions in Yeast

Neda Savic,\* Shawn P. Shortill,\* Misha Bilenky,<sup>†</sup> Joseph M. Dobbs,\* David Dilworth,\* Martin Hirst,<sup>†</sup>  
and Christopher J. Nelson\*<sup>1</sup>

\*Department. Biochemistry and Microbiology, University of Victoria, BC V8W 3P6, Canada and <sup>†</sup>BC Cancer Agency Genome Sciences Centre and the Department of Microbiology & Immunology, Michael Smith Laboratories, University of British Columbia, Vancouver, BC V6T 1Z3, Canada

ORCID IDs: 0000-0001-8742-7442 (S.P.S.); 0000-0002-4123-2209 (J.M.D.)

**ABSTRACT** Gene duplications increase organismal robustness by providing freedom for gene divergence or by increasing gene dosage. The yeast histone chaperones *Fpr3* and *Fpr4* are paralogs that can assemble nucleosomes *in vitro*; however, the genomic locations they target and their functional relationship is poorly understood. We refined the yeast synthetic genetic array approach to enable the functional dissection of gene paralogs. Applying this method to *Fpr3* and *Fpr4* uncovered redundant, cooperative, and divergent functions. While *Fpr3* is uniquely involved in chromosome segregation, *Fpr3* and *Fpr4* cooperate to regulate genes involved in polyphosphate metabolism and ribosome biogenesis. We find that the TRAMP5 RNA exosome is critical for fitness in  $\Delta fpr3\Delta fpr4$  yeast and leverage this information to identify an important role for *Fpr4* at the 5' ends of protein coding genes. Additionally, *Fpr4* and TRAMP5 negatively regulate RNAs from the nontranscribed spacers of ribosomal DNA. Yeast lacking *Fpr3* and *Fpr4* exhibit a genome instability phenotype at the ribosomal DNA, which implies that these histone chaperones regulate chromatin structure and DNA access at this location. Taken together, we provide genetic and transcriptomic evidence that *Fpr3* and *Fpr4* operate separately, cooperatively, and redundantly to regulate a variety of chromatin environments.

**KEYWORDS** chromatin; paralog; histone chaperone; genetic interactions; nucleolus

**G**ENE duplication events play an important role both in driving protein evolution and in providing a mechanism for ensuring the robustness of biological systems. Since the earliest observations of duplications on chromosomes (Darlington and Moffett 1930; Bridges 1936) and redundant genes (Kataoka *et al.* 1984; Basson *et al.* 1986), models implicating gene duplication events as complex drivers of evolution have been proposed (Ohno 1970; Hughes 1994; Force *et al.* 1999; Francino 2005; Innan and Kondrashov 2010). Evolutionary forces can favor the retention of redundant

genes for dosage reasons; for example, identical copies of histone and ribosomal genes are present in most eukaryotes. Alternately, duplicated genes provide an opportunity for functional divergence of gene pairs, or paralogs, over time.

The *FPR3* and *FPR4* genes encode two *Saccharomyces cerevisiae* paralogs (Benton *et al.* 1994; Manning-Krieg *et al.* 1994; Shan *et al.* 1994; Dolinski *et al.* 1997) derived from a distant ancestral gene (Wolfe and Shields 1997; Kellis *et al.* 2004; Pemberton 2006). They code for highly similar proteins (58% identical and 72% similar in amino acid residues) with acidic N-terminal nucleoplasmin-like histone chaperone and C-terminal FK506-binding (FKBP) peptidyl-prolyl isomerase domains (Kuzuhara and Horikoshi 2004; Xiao *et al.* 2006; Park *et al.* 2014) (Figure 1A). Both proteins localize to the nucleus and are enriched in the nucleolus (Benton *et al.* 1994; Manning-Krieg *et al.* 1994; Shan *et al.* 1994; Huh *et al.* 2003). Notably, *Fpr3* and *Fpr4* interact with each other and share some common physical interactors (Krogan *et al.* 2006), including histones (Shan *et al.* 1994; Nelson *et al.* 2006; Xiao *et al.* 2006) and the *Nop53* ribosome biogenesis

Copyright © 2019 Savic *et al.*

doi: <https://doi.org/10.1534/genetics.119.302235>

Manuscript received July 30, 2019; accepted for publication October 3, 2019; published Early Online October 11, 2019.

Available freely online through the author-supported open access option.

This is an open-access article distributed under the terms of the Creative Commons Attribution 4.0 International License (<http://creativecommons.org/licenses/by/4.0/>), which permits unrestricted use, distribution, and reproduction in any medium, provided the original work is properly cited.

Supplemental material available at figshare: <https://doi.org/10.25386/genetics.9911312>.

<sup>1</sup>Corresponding author: Department of Biochemistry and Microbiology 3800 Finnerty Road University of Victoria Victoria, BC V8W 3P6. E-mail: [cjn@uvic.ca](mailto:cjn@uvic.ca)

factor (Sydorsky *et al.* 2005). Additionally, both *FPR3* and *FPR4* are multicopy suppressors of temperature sensitivity and mating defects resulting from the absence of the Tom1 E3 ubiquitin ligase (Utsugi *et al.* 1999; Davey *et al.* 2000), and both *Fpr3* and *Fpr4* are required for the degradation of the centromeric histone H3 variant *Cse4* (Ohkuni *et al.* 2014). Therefore, there is good evidence that *Fpr3* and *Fpr4* cooperate.

There is also evidence that these paralogs have separate functions. *Fpr3* has been identified as a regulator of chromosome dynamics at mitotic and meiotic centromeres. During meiosis, *Fpr3* enhances recombination checkpoint delay (Hochwagen *et al.* 2005) and prevents meiotic chromosome synapsis initiation at centromeres (Macqueen and Roeder 2009). To our knowledge, no reports describe similar data for *Fpr4*. Thus, *Fpr3* may have functionally diverged. By contrast, *Fpr4* can silence expression of a reporter at ribosomal DNA (rDNA) (Kuzuhara and Horikoshi 2004), but the degree to which *Fpr3* regulates rDNA has not been described. Additionally, *Fpr4* is involved in transcription induction kinetics through the isomerization of prolines on the amino tails of histones H3 and H4 (Nelson *et al.* 2006). Finally, microarray gene expression analysis of  $\Delta fpr3$  and  $\Delta fpr4$  yeast identified small changes in partially overlapping sets of mRNAs (up to fourfold changes in 385 and 161 genes, respectively) (Park *et al.* 2014).

Loss-of-function phenotypes and genetic interactions usually provide insight into gene function. For example, the *ASF1* and *RTT106* genes, encoding histone chaperones, display clear chromatin-related genetic interactions in synthetic genetic array (SGA) screens (Costanzo *et al.* 2010, 2016). We noted that the genetic interactomes of *FPR3* and *FPR4* contained few chromatin-related hits (Collins *et al.* 2007; Costanzo *et al.* 2010, 2016; Stirling *et al.* 2011; Milliman *et al.* 2012) and hypothesized that the high similarity of these paralogs could render them semiredundant, masking their genetic interactions.

Here, through a set of comprehensive genetic interaction screens designed for paralogs and a series of RNA-sequencing (RNA-seq) transcriptome surveys, we demonstrate that *Fpr3* and *Fpr4* operate separately, cooperatively, and redundantly. Unique genetic interaction profiles and differentially expressed genes demonstrate that these histone chaperones are not equivalent; for example, *Fpr3* appears uniquely involved in chromosome segregation. By contrast, shared genetic interactions of *FPR3* and *FPR4* with the SWI/SNF and ADA chromatin regulators predicted that *Fpr3* and *Fpr4* cooperate to regulate genes. The identification of polyphosphate metabolism and ribosome biogenesis genes as *Fpr3/4* targets confirms this prediction. We find that the TRAMP5 RNA exosome becomes critical for fitness in  $\Delta fpr3\Delta fpr4$  yeast, and leverage this information to perform a sensitized survey for *Fpr4*-regulated genomic loci. This strategy identified an important role for *Fpr4* at the 5' ends of protein coding genes as well as at the nontranscribed spacer regions of rDNA. Finally, we show that yeast lacking *Fpr3* and *Fpr4*

exhibit a genome instability phenotype at the rDNA, implying that these histone chaperones regulate chromatin structure at these regions. Taken together we provide genetic and transcriptomic evidence that *Fpr3* and *Fpr4* operate separately, cooperatively, and redundantly to regulate a variety of chromatin environments.

## Materials and Methods

### Yeast strains and plasmids

Yeast strains used in this study are described in Supplementary Material, Appendix 5. Strains in the *MATa* nonessential yeast deletion mutant array (DMA) collection used for the SGA analysis are all isogenic to BY4741 and were purchased from Thermo Fisher Dharmacon. The plasmid rescued double genomic deletion  $\Delta fpr3\Delta fpr4$  SGA query strain (YNS 35) was created in a Y7092 genetic background as follows. The endogenous *FPR4* locus on a Y7092 wild-type strain was replaced with a nourseothricin resistance (*MX4-NATR*) PCR product deletion module. The resulting single-gene  $\Delta fpr4$  deletion mutant was subsequently transformed with prs316 *FPR4*: a single-copy, *URA3*-marked shuttle vector carrying an untagged, full-length copy of the *FPR4* open reading frame with endogenous promoter and terminator [originally described in Nelson *et al.* (2006)]. The endogenous *FPR3* locus on this plasmid-rescued  $\Delta fpr4$  deletion mutant was subsequently replaced with a *LEU2* PCR product deletion module.

Triple deletion mutants  $\Delta trp6\Delta fpr3\Delta fpr4$  and  $\Delta trf5\Delta fpr3\Delta fpr4$  and their corresponding mixed-population total haploid meiotic progeny controls used in the validating growth curves were generated from the SGA cross (see below).

Single-gene deletion mutants of  $\Delta fpr3$ ,  $\Delta fpr4$ , and  $\Delta sir2$  used for the RNA-seq are all isogenic to BY4741 and were either purchased from open biosystems or taken from the yeast DMA (purchased from Thermo Fisher Dharmacon). The isogenic double deletion  $\Delta fpr3\Delta fpr4$  mutant was constructed from the open biosystems  $\Delta fpr3$  single-gene deletion mutant by replacing the endogenous *FPR4* locus with a nourseothricin resistance (*MX4-NATR*) PCR product deletion module. The *FPR4*( $\Delta fpr3\Delta trf5$ ) and  $\Delta fpr3\Delta fpr4\Delta trf5$  isogenic strains and their corresponding total haploid mixed-population controls were generated from the SGA cross (see below).

### SGA analysis

SGA analysis was performed using a Singer Instruments ROTOR microbial arraying robot as previously described (Tong and Boone 2006), with the following modifications. The *MATa*/ $\alpha$  diploid zygotes resulting from the query strain DMA cross were pinned onto diploid selective YPD + G418/clonNAT plates a total of two times for greater selection against any residual haploids. Sporulation was carried out at room temperature for 14 days. Spores were pinned onto *MATa* selective germination media for two rounds of selection as previously described (Tong and Boone 2006).

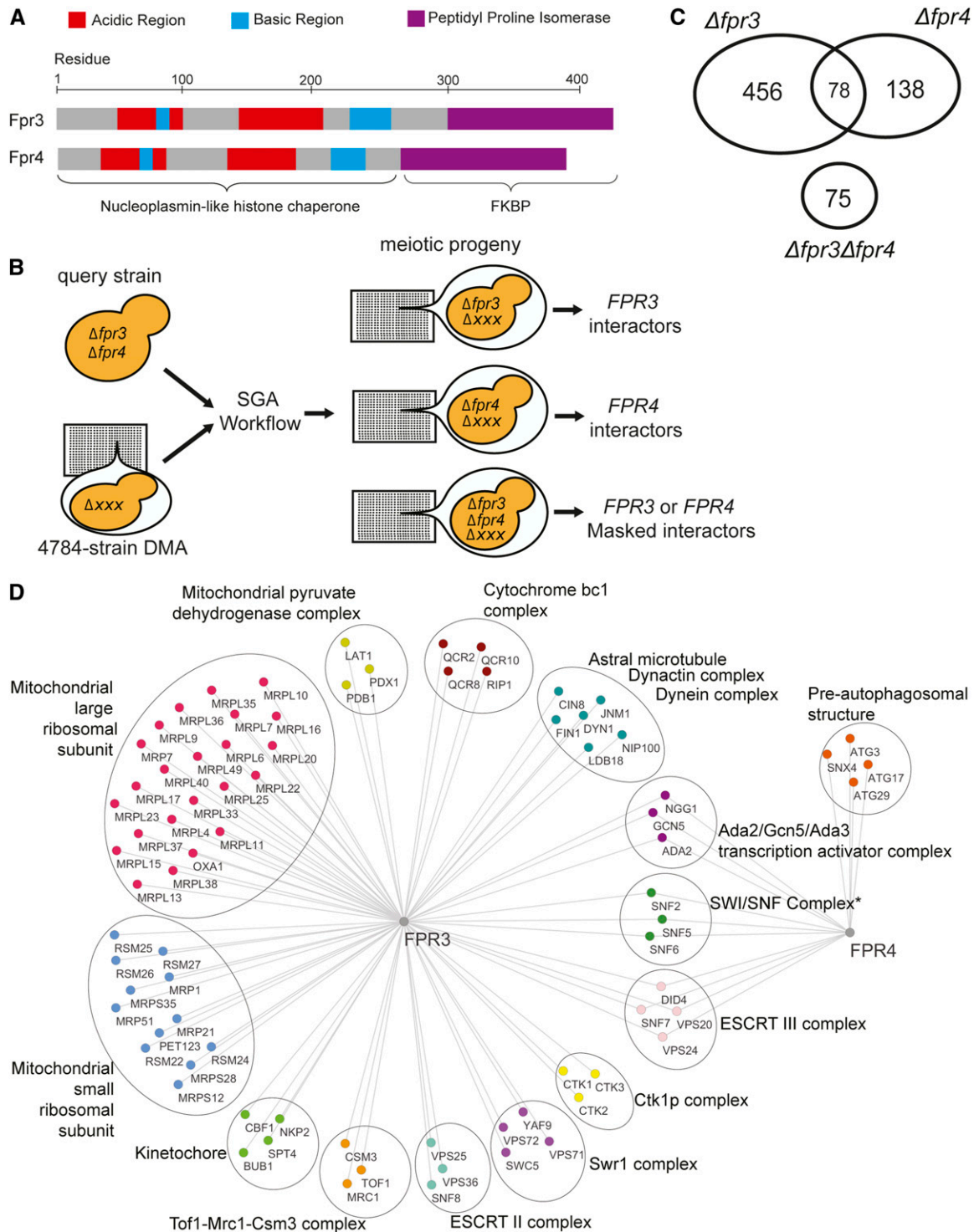


**Figure 1** *Fpr3* and *Fpr4* have separate, cooperative, and redundant functions. (A) Domain architectures of *Fpr3* and *Fpr4*. Both proteins have an N-terminal nucleoplasmin-like domain with characteristic patches of acidic and basic residues, and a C-terminal FK506-binding (FKBP) peptidyl prolyl isomerase domain. (B) Schematic illustrating modified paralogue-SGA workflow. Spores from a single cross of the double deletion  $\Delta fpr3 \Delta fpr4$  query to the 4784 strain DMA are manipulated to generate three separate sets of meiotic progeny for interactome analysis. The query strain also harbored an episomal *URA3* plasmid with a functional *FPR4* gene to avoid the slow growth phenotype of  $\Delta fpr3 \Delta fpr4$  dual deletion, and its vulnerability to suppressor mutations. This plasmid was selected for (for *FPR3* interactors) or against (for *FPR4* interactors) in the last step of the screen. (C) Venn diagram illustrating shared and unique negative genetic interactions from  $\Delta fpr3$  and  $\Delta fpr4$  paralogue-SGA screens. The number of negative genetic interactions only detectable in double deletion  $\Delta fpr3 \Delta fpr4$  mutants is represented below. (D) Network illustrating complex related ontologies enriched among unique and shared negative genetic interactors of *FPR3* and *FPR4*. \* *SNF2*, *SNF5*, and *SNF6* were identified as hits in the *FPR4* screen only, but displayed a synthetically sick phenotype with both  $\Delta fpr3$  and  $\Delta fpr4$  mutations in confirmatory spotting assays (not shown).

The resulting *MATa* progeny were subsequently replica plated onto four kinds of selective media: control media selective for the total haploid meiotic progeny population (SD media lacking histidine, arginine, and lysine, and containing canavanine and thialysine both at a final concentration of 50 mg/liter, and G418 at a final concentration of 200 mg/liter), media selective for  $\Delta xxx\Delta fpr3$  haploid meiotic progeny (SD media lacking histidine, arginine, lysine, leucine, and uracil, and containing canavanine and thialysine both at a final concentration of 50 mg/liter, G418 and clonNAT both at a final concentration of 200 mg/liter), media selective for  $\Delta xxx\Delta fpr4$  haploid meiotic progeny (SD media lacking histidine, arginine, and lysine, and containing canavanine and thialysine both at a final concentration of 50 mg/liter, G418 and clonNAT both at a final concentration of 200 mg/liter, and 5-fluoroorotic acid (5-FOA) at a final concentration of 1000 mg/liter), and finally, media selective for  $\Delta xxx\Delta fpr3\Delta fpr4$  haploid meiotic progeny (SD media lacking histidine, arginine, lysine, and leucine, and containing canavanine and thialysine both at a final concentration of 50 mg/liter, G418 and clonNAT both at a final concentration of 200 mg/liter, and 5-FOA at a final concentration of 1000 mg/liter). Plates were incubated at 30° for 24 hr and were then expanded into triplicate and incubated for an additional 24 hr at 30°.

Images of each plate were scanned and subsequently processed using the Balony image analysis software package as previously described (Young and Loewen 2013). In brief, pixel area occupied by each colony was measured to determine colony size. Progeny fitness was then scored as follows. The ratio of each double ( $\Delta xxx\Delta fpr3$ ,  $\Delta xxx\Delta fpr4$ ) and triple ( $\Delta xxx\Delta fpr3\Delta fpr4$ ) mutant colony size relative to its corresponding total haploid meiotic progeny control colony was determined. Ratio cut-off thresholds were estimated automatically by the software by extrapolating the central linear portion of the ratio distributions and finding the *y*-intercepts at either ends of the *x*-axis. Genetic interactions were identified using the automatically estimated upper and lower cut-off thresholds and default Balony hit parameters (*i.e.*, reproducibility in 3/3 sets and *P*-values < 0.05) (a complete list of all genetic interactions generated from each data set is presented in Appendix 1).

### SGA data processing

Unique, common, and masked synthetic sick/lethal interactors were identified as follows. First, duplicate genes in the lists of hits from each data set were removed. The three lists of hits were then compared to each other. The  $\Delta fpr3$  and  $\Delta fpr4$  screens were compared to identify unique and common interactors. Genes uniquely present in the  $\Delta fpr3\Delta fpr4$  double mutant screens were defined as masked interactors. Unique, common, and masked suppressor interactors were identified the same way.

The lists of unique, common, and masked synthetic sick/lethal and suppressor genetic interactors were subsequently analyzed using the web based FunSpec bioinformatics tool (<http://funspec.med.utoronto.ca/>, Dec 2017). The analysis

was performed using a *P*-value cut-off score of 0.01, and without Bonferroni correction. A full list of the ontologies uncovered and their corresponding *P*-values are presented in Appendix 2. Networks illustrating the unique and common complex related genetic interactions were drawn using the Cytoscape software platform (<http://www.cytoscape.org/>).

### Growth curves

Growth curves to validate the synthetic sickness phenotypes were carried out as follows. Colonies generated from the SGA assay corresponding to each triple mutant of interest and its respective control colony were isolated and validated for correct genotype by PCR. Confirmed strain isolates were then resuspended in fresh YPD media, normalized to an OD<sub>600</sub> of 0.2 and distributed into triplicate wells of a 24-well cell culture plate. Plates were subsequently grown for 16 hr at 30° in a shaking plate reader. Readings of OD<sub>600</sub> were taken every 30 min.

### RNA-seq library preparation and sequencing

Single colony isolates of each strain were grown to midlog phase in 50 ml of liquid YPD media. Samples were then pelleted and washed once with sterile water before being flash frozen in liquid nitrogen and stored for 16 hr at -80°. Samples were thawed on ice, and RNA was extracted using a phenol freeze-based approach as previously described (Schmitt *et al.* 1990). The extracted RNA was subsequently treated with RNase-free DNase I (Thermo Fisher Scientific).

RNA samples were processed and sequenced at the BC Cancer Agency Michael Smith Genome Sciences Centre following standard operating protocols. Briefly, total RNA samples were ribo-depleted using the Ribo-Zero Gold rRNA Removal Kit (Yeast) (Illumina, San Diego, CA) and analyzed on an Agilent 2100 Bioanalyzer using Agilent 6000 RNA Nano Kit (Agilent Technologies, Santa Clara, CA). Complementary DNA (cDNA) was generated using the Superscript Double-Stranded cDNA Synthesis kit (Thermo Fisher) and 100 bp paired-end libraries were prepared using the Paired-End Sample Prep Kit (Illumina).

### Processing of sequencing data

Sequenced paired-end reads were aligned to the *sacCer3* reference genome ([https://www.ncbi.nlm.nih.gov/assembly/GCF\\_000146045.2/](https://www.ncbi.nlm.nih.gov/assembly/GCF_000146045.2/)) using the BWA aligner (Li and Durbin 2010) (version 0.6.1-r104-tpx). We observed that out of 5110 *S. cerevisiae* genes annotated in Ensembl v.90, only 267 are spliced with 251 having one intron. Therefore, we considered genomic alignment of RNA-seq reads as a good approximation for the yeast transcriptome analysis. For every library a total of ~1.5–2M reads were sequenced, of which ~75–95% of reads were aligned.

To quantify gene expression, we filtered reads that aligned to multiple locations (and therefore cannot be placed unambiguously) by applying a BWA mapping quality threshold of five. We further collapsed fragments that were duplicated (only counting a single copy of a read pair if a number of

pairs with the same coordinates was sequenced) and removed chastity failed reads, considering only reads that were properly paired. Postprocessing was performed using the “pysam” application for python (<https://github.com/pysam-developers/pysam>). The alignment statistics were calculated using the “sambamba” tool v.0.5.5 5 (Tarasov *et al.* 2015).

We considered cDNA fragment lengths distributions as well as genome-wide distributions of read coverage (data not shown) to ensure that these characteristics are similar for the pairs of data sets in the differential gene expression (DE) analysis. Genome-wide pair-ended fragment coverage profiles for both strands were generated, as well as read counts for every gene for further DE analysis.

The reads per kilobase per million values were calculated for every gene, and DE analysis was performed using the DEfine algorithm (M. Bilenky, unpublished data). First, the chi-squared *P*-value was estimated for every gene, under the null hypothesis that the gene is not differentially expressed between two data sets. The Benjamini–Hochberg false discovery rate control procedure was applied (false discovery rate = 0.05) to find a *P*-value threshold. To further reduce noise, we only considered genes with a fold change between reads per kilobase per million values of > 1.5, and required a minimal number of aligned reads of > 5 per gene. Only reads aligned to the proper strand were considered in the DE analysis.

In addition to the standard DE analysis, where gene expression quantification was done by counting reads falling into the gene boundaries, we considered a model-independent approach by calculating read counts in every 175-bp-long bin genome-wide (for both strands), and performed DE analysis between bins (with the same approach we used for genes, see above). After defining the DE bins, we overlapped their locations with gene coordinates to determine DE genes. This second approach also provided a list of potential differential gene-expressed intergenic regions. A full list of the DE genes is presented in Appendix 3.

#### **Quantitative real-time PCR validation of DE transcripts**

Total RNA was prepared from single colony isolates of each strain grown to midlog phase in 50 ml of liquid YPD media using a phenol freeze-based approach as previously described (Schmitt *et al.* 1990). The extracted RNA was subsequently treated with RNase-free DNase I (Thermo Fisher Scientific) and cDNA was prepared using a High-Capacity cDNA Reverse Transcription Kit (Applied Biosystems). Quantitative real time PCR was performed using the Maxima SYBR Green qPCR Master Mix (Thermo Scientific) and the forward and reverse primers are listed in Appendix 6. Experimental gene Ct values were normalized to the mean Ct values of two housekeeping gene normalizers: *TCM1* and *GPD1*.

#### **Ontology analysis of DE genes**

Ontologies associated with differentially expressed genes or genetic interactions were identified using the web-based

FunSpec bioinformatics tool (<http://funspec.med.utoronto.ca/>, Dec 2018). The analysis was performed on genes displaying a fold change of  $\geq 1.3$ , using a *P*-value cut-off score of 0.001, and with Bonferroni correction. A full list of the ontologies uncovered and their corresponding *P*-values is presented in Appendix 4.

#### **Averaged gene read maps**

Universal gene coverage profiles were generated as follows: we first created cDNA fragment coverage profiles genome-wide for both strands using all aligned read pairs. Next, we selected profiles for individual genes and scaled them to 100 units and normalized by the total gene coverage. After that, we agglomerated all scaled and normalized gene coverage profiles together. When doing this, the profiles for genes on the negative strand were inverted (in other words, we always agglomerated profiles from 5' to 3' of the gene).

#### **rDNA reporter propagation assays**

The URA<sup>+</sup> status of each reporter containing strain was first confirmed by growth on SD media lacking uracil. Saturated overnights were then prepared from single colony isolates of each confirmed strain in liquid YPD media. Cultures were prepared from the overnights in 50 ml YPD media and grown at 30° to midlog phase. Cells were subsequently collected, washed once, resuspended in sterile deionized water, and normalized to an OD<sub>600</sub> = 0.5. Normalized cell suspensions were subsequently diluted 10-fold and 250  $\mu$ l of each dilution was plated on 25 ml SD 5-FOA plates. Plates were incubated at 30° for 16 hr. A total of 96 well-isolated colonies were randomly picked from each 5-FOA plate using the Genetix QPix-2 colony picking robot, and deposited onto nonselective solid YPD plates. Plates were incubated for 5 days at 30°. All 96 colonies on each YPD plate were then replica-plated onto SD complete control media and SD media lacking uracil, and incubated for 5 days at 30° before being imaged.

#### **Data availability statement**

Appendix 1 contains lists of all genetic interactions detected in this study. Appendix 2 contains the gene ontology analysis of genetic interactions. Appendix 3 contains lists of all differentially expressed genes detected in this study. Appendix 4 contains the gene ontology analysis of differentially expressed genes. RNA-seq data are deposited in the Gene Expression Omnibus Repository (accession number GSE134075). All yeast strains and primers used in this study are listed in Appendices 5 and 6, respectively. Supplemental material available at figshare: <https://doi.org/10.25386/genetics.9911312>.

## **Results**

### **Genetic interactions reveal separate, cooperative, and redundant functions of FPR3 and FPR4**

Since  $\Delta fpr3$  and  $\Delta fpr4$  yeast are viable but double  $\Delta fpr3\Delta fpr4$  mutants display a synthetic sick phenotype (Dolinski *et al.*

1997; Costanzo *et al.* 2010), we reasoned that partial redundancy may be masking genetic interactions. To address this and determine the biological processes sensitive to these histone chaperones, we performed a modified SGA screen designed to dissect functional redundancy of gene paralogs (Figure 1B, see *Materials and Methods*). To this end, we crossed a dual-query  $\Delta fpr3\Delta fpr4$  double mutant strain to the 4784 strain nonessential yeast DMA, so that the fitness of all double ( $\Delta fpr3\Delta xxx$  and  $\Delta fpr4\Delta xxx$ ) and triple ( $\Delta fpr3\Delta fpr4\Delta xxx$ ) mutant meiotic progeny could be measured in parallel. The query strain also harbored an episomal *URA3* plasmid with a functional *FPR4* gene to avoid the slow growth phenotype of  $\Delta fpr3\Delta fpr4$  dual deletion yeast, and its vulnerability to suppressor mutations. This plasmid was maintained until the final step of the screen, when counterselection with 5'FOA created the *fpr4* null status. Using standard selection methods, the spores of this single cross were manipulated to generate three separate SGA screens that identified all genetic interactions with  $\Delta fpr3$ ,  $\Delta fpr4$ , and genes whose disruption affected the fitness of yeast lacking both  $\Delta fpr3\Delta fpr4$ .

We identified 456 and 138 genetic interactors that were unique to either *FPR3* or *FPR4*, respectively, revealing that these paralogs are not equivalent (Figure 1C, top). An additional 78 genes interacted with both *FPR3* and *FPR4*, implying that there are specific contexts of paralog cooperativity; that is, situations where both histone chaperones are required for function. We also uncovered 75 masked interactors, defined as genes whose deletion only affects the fitness  $\Delta fpr3\Delta fpr4$  yeast (Figure 1C, bottom). These genes highlight processes where paralog function is redundant. The complete list of these genes and a gene ontology analysis are provided in Appendices 1 and 2, respectively.

*FPR3* genetic interactors fall into a diverse collection of protein complex ontologies, including members of the large and small mitochondrial ribosomal subunits ( $P < 10^{-14}$  and  $P = 7.49 \times 10^{-7}$ , respectively), the mitochondrial pyruvate dehydrogenase complex ( $P = 1.16 \times 10^{-3}$ ), the cytochrome bc1 complex ( $P = 3.11 \times 10^{-3}$ ), and components of the ESCRT II endosomal sorting complex ( $P = 3.06 \times 10^{-4}$ ) (Figure 1D). We also identified all three components of the Ctk1 kinase complex ( $P = 3.06 \times 10^{-4}$ ) and four components of the Swr1 chromatin remodeler ( $P = 9.00 \times 10^{-3}$ ), supporting at least some potential chromatin-centric roles of *Fpr3*. Most notably, we uncovered complexes involved in chromosome segregation such as the astral microtubule ( $P = 6.48 \times 10^{-6}$ ), kinetochore ( $P = 1.14 \times 10^{-4}$ ), and the *Mrc1/Csm3/Tof1* complex ( $P = 3.06 \times 10^{-4}$ ) as genetic interactors unique to *Fpr3*, and not *Fpr4*. These systems-level data support reports indicating that *Fpr3*, but not *Fpr4*, regulates mitotic and meiotic chromosome dynamics, including those associated with centromeres (Hochwagen *et al.* 2005; Macqueen and Roeder 2009; Ohkuni *et al.* 2014). Although we identified 138 *FPR4*-specific genetic interactions, they fall into limited ontologically related protein complex categories. Several genes coding for

components of the preautophagosome and associated with the process of mitochondrion degradation ( $P = 2.89 \times 10^{-3}$ ) were the exception, but the relationship between *Fpr4* and this process is not clear. Taken together, the number and nature of negative genetic interactions from single-query screens suggest that *Fpr4* cannot fulfill many of the biological functions of *Fpr3*, particularly those in chromosome dynamics and mitochondrial ribosome biology. However, *Fpr3* might be able to substitute for *Fpr4* (see below).

Shared genetic interactions would be expected if both paralogs were required for the efficient execution of a biological process. Among genetic interactors common to both *FPR3* and *FPR4* are genes coding for the ESCRT III complex ( $P = 6.05 \times 10^{-6}$ ), which functions in endosomal sorting; the *Ada2/Gcn5/Ada3* histone acetyltransferase ( $P = 1.50 \times 10^{-5}$ ); and the ATP-dependent SWI/SNF chromatin remodeler (Figure 1D). Shared genetic interactions with the SWI/SNF remodeler were confirmed using spotting assays (data not shown). The proposed cooperation of *Fpr3* and *Fpr4* is supported by the fact these proteins copurify (Krogan *et al.* 2006) and, like nucleoplasmin, have the intrinsic propensity to form oligomers (Dutta *et al.* 2001; Edlich-Muth *et al.* 2015; Koztowska *et al.* 2017). Thus, these shared genetic interactions with known chromatin regulatory complexes support published protein complex data and indicate that *Fpr3* and *Fpr4* likely cooperate in some contexts.

A total of 75 masked genetic interactions are only detectible in double  $\Delta fpr3\Delta fpr4$  mutants (Figure 1C, bottom). These genes are essential only when both paralogs are absent, and thus highlight processes in which *Fpr3* and *Fpr4* are redundant. Most notably these interactors include *TRF5* and *AIR1* (Figure 2A), two nonessential components of the TRAMP5 nuclear RNA exosome, an RNA surveillance factor that recognizes, polyadenylates, and degrades aberrant RNA transcripts (Figure 2B) (LaCava *et al.* 2005; Houseley and Tollervey 2008; San Paolo *et al.* 2009; Wery *et al.* 2009). An additional nonessential subunit of the nuclear RNA exosome (*RRP6*) was at the threshold of significance, using default Balony settings (Figure 2A). We independently confirmed synthetic sickness of  $\Delta fpr3\Delta fpr4$  with  $\Delta trf5$  and  $\Delta rrp6$ , using growth curves (Figure 2C). Negative genetic interactions with three nonessential components of the TRAMP5 exosome strongly suggests that *Fpr3* and *Fpr4* have redundant biological functions likely involving the negative regulation of RNAs.

### Suppressor genetic interactions of *FPR3* and *FPR4*

The SWI/SNF and ADA complexes are particularly important for the fitness of  $\Delta fpr3$  and  $\Delta fpr4$  yeast (Figure 1D). In support of a chromatin defect underlying these phenotypes, we found that several genetic suppressors (Figure 3) that alleviate the slow growth phenotype of  $\Delta fpr3\Delta fpr4$  yeast are themselves chromatin modifiers. These include *Hos2*, *Hda1*, and *Hos3*, three NAD<sup>+</sup> independent histone deacetylases ( $P = 6.33 \times 10^{-5}$ ); *Hir1*, *Hpc2*, and *Hir3*, three of the four components of the HIR replication-independent

nucleosome assembly complex ( $P = 1.29 \times 10^{-5}$ ); and *Swd3* and *Sdc1*, two of the eight components of the *Set1/COMPASS* histone H3K4 methylase complex ( $P = 5.87 \times 10^{-3}$ ). We note that the *Swd2* subunit of *COMPASS* is encoded by an essential gene and the *Δset1* knockout is not present in our deletion strain collection. It is particularly notable that we find histone deacetylases enriched among suppressor interactions and histone acetyltransferases among synthetic sick and lethal interactions. The presence of both aggravating and alleviating chromatin-related genetic interactions in our modified SGA screen is consistent with a chromatin-centric mode of action for *Fpr3* and *Fpr4*.

### ***Fpr3* and *Fpr4* regulate partially overlapping sets of genes**

The genetic interactions of *Fpr3* and *Fpr4* with known chromatin modifiers suggest that they regulate transcription. Indeed a microarray study determined these histone chaperones regulate the expression of a broad set of functionally diverse protein coding genes (Park *et al.* 2014). Because these experiments did not include an analysis of *Δfpr3Δfpr4* double mutants and were restricted to protein coding regions of the genome, we sought to obtain a more complete view of the effects of *Fpr3* and *Fpr4* on the transcriptome. To this end, we performed a singlicate RNA-seq survey screen of the ribonucleic acid fraction of RNAs from wild-type, *Δfpr3*, *Δfpr4*, and *Δfpr3Δfpr4* yeast (Figure 4, A and B). To verify this survey approach, we included a *Δsir2* strain as a control, which in our analysis displayed 854 differentially expressed genes (Figure 4A), using a lenient cut-off of 1.3-fold (a similar threshold to that of Park *et al.* (2014)). The number and nature of *Sir2*-regulated genes we identified is in good agreement with previous reports of *Sir2*-regulated genes and binding sites (Li *et al.* 2013; Ellahi *et al.* 2015). A complete list of differential expressed genes from these experiments can be found in Appendix 3.

Single deletion mutants of *Δfpr3* and *Δfpr4* had 529 and 549 differentially expressed genes, respectively (Figure 4A, Appendix 3). Two general observations are consistent with previous microarray analyses (Park *et al.* 2014). First, roughly one-third of *Fpr3*-regulated transcripts are also regulated by *Fpr4*, and vice versa, confirming that on these genes, transcriptional regulation requires cooperation between paralogs (Figure 4B). Second, the effect of these histone chaperones on gene expression can be positive or negative, but the effect of *Fpr3* and *Fpr4* is always in the same direction. Since approximately two-thirds of differentially expressed genes were downregulated (Figure 4, A and B, blue), these histone chaperones appear to predominantly promote gene expression.

To determine if *Fpr3* and *Fpr4* have distinct effects on the transcriptome, we subjected the gene lists represented by sectors in Figure 4B to gene ontology analysis. While the singlicate nature of our comparative RNA-seq approach means the interpretation of DE genes should be taken with

caution, it is noteworthy that genes uniquely regulated by *Fpr3* and *Fpr4* appear to fall into functionally distinct categories (Appendix 4). The 337 *Fpr3*-regulated genes retrieved the term transferase activity ( $P = 2.11 \times 10^{-7}$ ) and the generic term of metabolic process ( $P = 1.99 \times 10^{-5}$ ), while *Fpr4*-regulated genes are enriched in RNA-binding functions ( $P = 7.69 \times 10^{-6}$ ), nucleotide-binding functions ( $P = 1.91 \times 10^{-5}$ ), ribosome biogenesis processes ( $P = 1.07 \times 10^{-11}$ ), and rRNA processing processes ( $P = 8.51 \times 10^{-9}$ ). A total of 338 genes were uniquely misregulated in *Δfpr3Δfpr4* double mutants, but these genes generally fall into previously described *Fpr3* and *Fpr4* categories, including transferase activity ( $P = 4.45 \times 10^{-5}$ ) and rRNA binding ( $P = 4.99 \times 10^{-4}$ ). Taken together, these results indicate that *Fpr3* and *Fpr4* have nonoverlapping effects on a fraction of the transcriptome, but may be functionally redundant on some genes.

We identified 127 genes (62 upregulated, 65 downregulated) that are differentially expressed in all three RNA-seq libraries (*Δfpr3*, *Δfpr4*, and *Δfpr3Δfpr4*). Genes downregulated in all three experiments are enriched in factors involved in iron siderophore transport ( $P = 4.33 \times 10^{-9}$ ). We found that the 62 upregulated genes are highly enriched in ribosomal protein genes ( $P = 5.07 \times 10^{-8}$ ) and factors involved in phosphate transport ( $P = 1.24 \times 10^{-6}$ ) and polyphosphate metabolism ( $P = 4.20 \times 10^{-7}$ ). In fact, the most differentially expressed genes in our survey (up to 60-fold upregulated) are phosphate metabolic genes such as *PHO5* and *PHO11/12*, encoding acid phosphatases; and *PHO89*, *PHO84*, and *PIC2*, encoding phosphate transporters. Since previous studies did not identify the *PHO* genes as *Fpr3/4*-regulated, we verified our RNA-seq observations using independent biological replicates and quantitative real-time PCR of two *PHO* genes (Figure 4C), as well as one downregulated siderophore transporter, *SIT1*. The identification of polyphosphate metabolism and ribosomal protein genes as *Fpr3/4* targets is noteworthy given a recent report that identified *Fpr3* and *Fpr4* as major direct targets of protein polyphosphorylation, and established conserved links between the polyphosphorylation and ribosome biogenesis network in yeast and human cells (Bentley-DeSousa *et al.* 2018).

In summary, our RNA-seq experiments demonstrate that *Fpr3* and *Fpr4* have nonoverlapping effects on the transcriptome. Most significantly, we find that both paralogs are required for repression of genes involved in phosphate uptake and polyphosphate metabolism, as well as ribosomal protein genes.

### **The *TRAMP5* RNA exosome masks the effects of *Fpr4* on transcription**

Deletion of *TRF5*, encoding the defining component of the *TRAMP5* nuclear RNA exosome, induces severe sickness in *Δfpr3Δfpr4* yeast (Figure 2). We therefore wondered whether *TRAMP5* might be required for the degradation of transcripts negatively regulated by these paralogs. To test this idea, we focused on *Fpr4*-regulated genes by sequencing

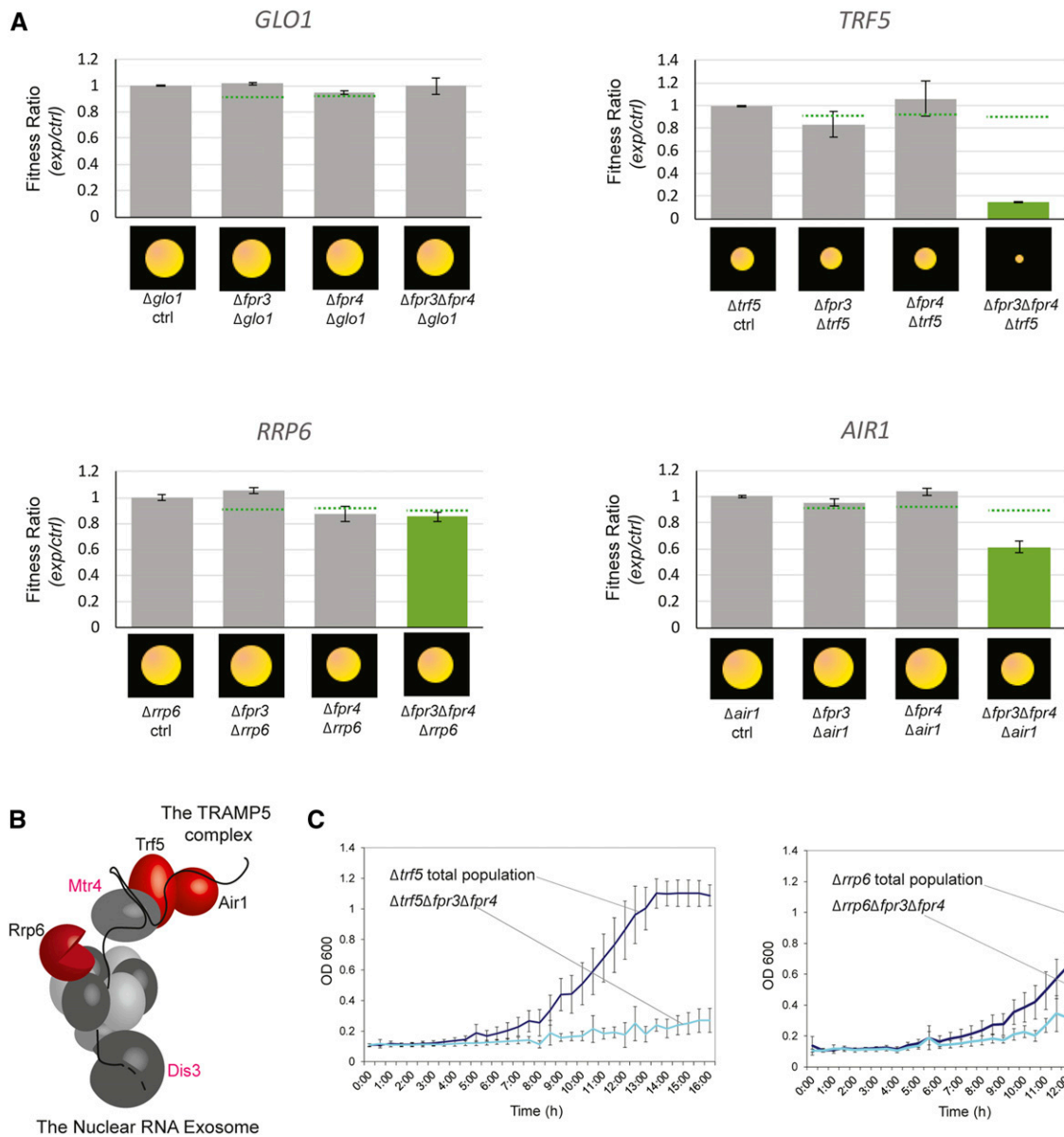


**Figure 2** The TRAMP5 nuclear RNA exosome is a masked genetic interactor of *FPR3* and *FPR4*. (A) Fitness ratios of the indicated single, double, and triple mutants generated from parallel-SGA screens. The mean colony size ratios of  $\Delta fpr3 \Delta xxx$ ,  $\Delta fpr4 \Delta xxx$ , and  $\Delta fpr3 \Delta fpr4 \Delta xxx$  mutants relative to colony sizes of  $\Delta xxx$  total haploid meiotic progeny are plotted as histograms. Ratios significantly below the default cut-off threshold (dotted green line) are indicated with green bars. A Balony software-generated image of the mean colony size of each mutant, normalized to the plate median colony size, is illustrated along the x-axis. *GLO1* is a negative control that does not display a genetic interaction in  $\Delta fpr3 \Delta$ ,  $\Delta fpr4 \Delta$ , or  $\Delta fpr3 \Delta fpr4$  screens. (B) A schematic of the TRAMP5 complex (top right) interacting with the nuclear RNA exosome (bottom left). Genetic interactors identified in A are colored red. Pink text indicates essential components. Illustration is adapted from (Wolin et al. (2012)). (C) Growth curves for select triple deletion mutants and corresponding total haploid meiotic progeny control populations confirm the slow growth of  $\Delta fpr3 \Delta fpr4 \Delta trf5$  and  $\Delta fpr3 \Delta fpr4 \Delta rrp6$  mutants.

the ribo-minus transcriptomes of two strains from our SGA screen:  $\Delta trf5$  haploids with a functional *Fpr4* ( $\Delta fpr3 \Delta trf5$ ), and isogenic haploids from the same spores that lack both *Fpr3/4* proteins ( $\Delta fpr3 \Delta fpr4 \Delta trf5$ ). This provided a sensitized approach to reveal *Fpr4*-regulated RNAs because functional compensation by *Fpr3* is not possible and potential degradation of upregulated RNAs by TRAMP5 is eliminated. This comparison ( $\Delta fpr3 \Delta trf5$  vs.  $\Delta trf5 \Delta fpr3 \Delta trf5$ ) uncovered a total of 1321 differentially expressed genes (967 upregulated and

354 downregulated) (Figure 4D). A summary of gene ontology analysis of upregulated genes is provided in Figure 4E. Genes encoding protein components of the cytosolic ribosome ( $P = 3.21 \times 10^{-12}$ ) and genes associated with rRNA processing ( $P = 1.14 \times 10^{-8}$ ) are highly enriched as *Fpr4* targets. Also enriched were genes coding for constituents of the fungal-type cell wall ( $P = 1.87 \times 10^{-4}$ ) and the electron transport chain ( $P = 6.12 \times 10^{-8}$ ) (Figure 4E). These results partially explain the underestimation of genes negatively  $\Delta fpr4$  transcriptomes

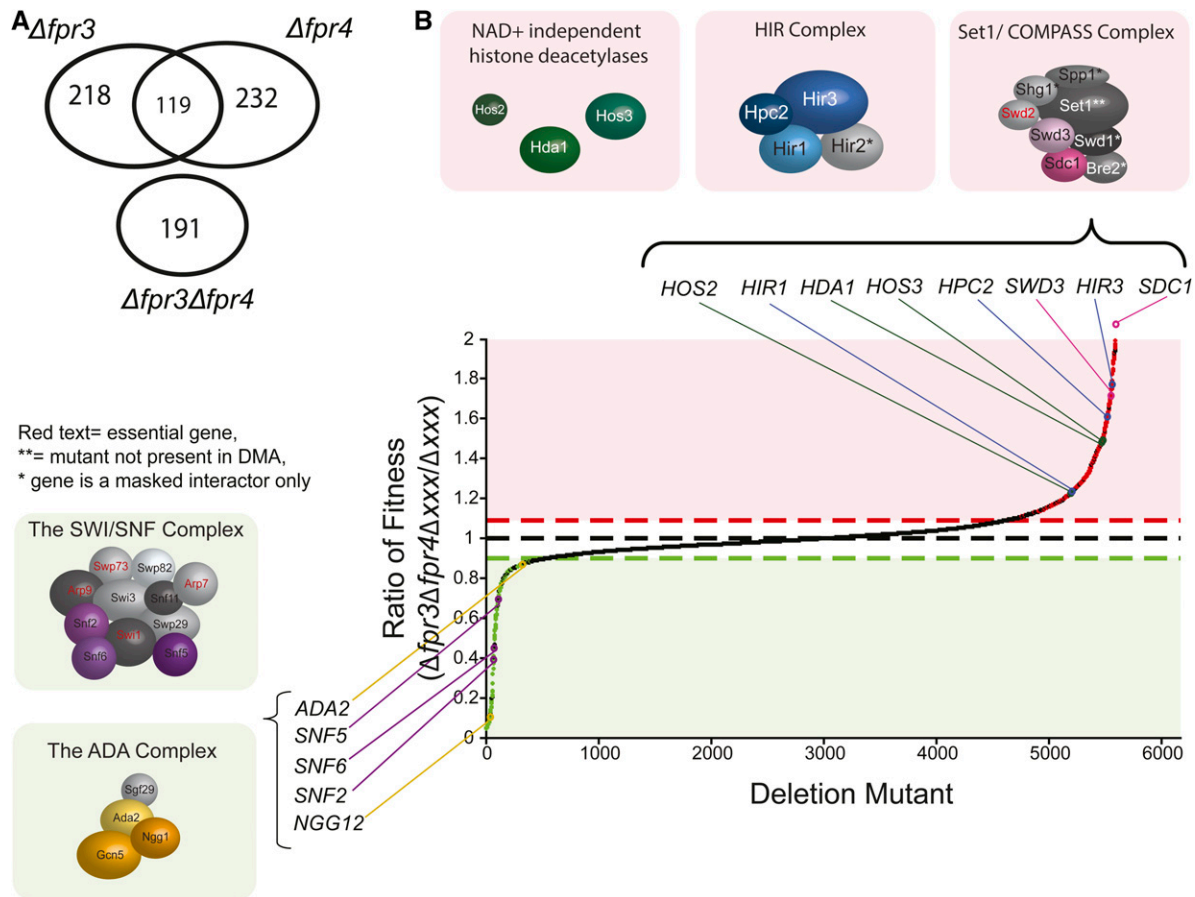


**Figure 3** Suppressor genetic interactions support chromatin-centric functions for *Fpr3* and *Fpr4*. (A) Venn diagram illustrating shared and unique suppressor interactors from  $\Delta fpr3$  and  $\Delta fpr4$  paralogue-SGA screens. The number of suppressor genetic interactions only detectable in double deletion  $\Delta fpr3\Delta fpr4$  mutants is represented below. (B) Plot of fitness ratios for all  $\Delta fpr3\Delta fpr4\Delta xxx$  triple mutants relative to  $\Delta xxx$  total haploid meiotic progeny controls. Green dots indicate negative genetic interactions, red dots indicate all suppressor genetic interactions. Threshold cut-offs are indicated by red and green dashed horizontal lines. The location of significant hits coding for components of chromatin modifiers are labeled and accompanied with schematic illustrations of their complex components. Components coded for by paralogue-SGA hits are colored. Red text denotes essential complex components.

(Figure 4A). That is, the TRAMP5 RNA exosome may buffer changes in the levels of some *Fpr4* regulated RNAs.

#### A signature of incomplete elongation is present in $\Delta fpr4$ yeast

Further interrogation of our transcriptome data reveals additional evidence for *Fpr4* in the regulation of transcription: we noticed that a significant proportion (~40%) of differentially expressed genes in  $\Delta fpr3\Delta fpr4\Delta trf5$  yeast displayed an accumulation of reads toward the 5' end of the annotated transcript. Subsequent bioinformatic analysis of the total transcriptomes of  $\Delta fpr3\Delta fpr4\Delta trf5$  and  $\Delta fpr3\Delta trf5$  mutants revealed that this asymmetry (or 5'-bias) is widespread, and detectable in genes, irrespective of their net change in transcription (Figure 5A). RNA-seq reads on two example genes illustrating this asymmetry signature are presented in Figure 5B; *SSF1* codes for a constituent of the 66S preribosome and is required for large ribosomal subunit maturation, while *UTP9* codes for a component required for proper endonucleolytic cleavage of 35S rRNA.

The paired-end tag coverage on both of these genes, but not the *ACT1* gene (Figure 5C), displays the characteristic 5' asymmetry in  $\Delta fpr3\Delta fpr4\Delta trf5$  yeast. We verified these observations using independent biological replicates and quantitative real-time PCR using 5' and 3' amplicons of *UTP9* and *SSF1*, which were normalized to the unchanged *GPD1* gene (Figure 5D). This transcriptome signature demonstrates three novel findings: first, *Fpr4* negatively regulates transcription from many genes even though total reads per gene may not change; second, *Fpr4* action is critical at a stage after initiation, likely transcriptional elongation; and third, because this signature of accumulated 5' reads on genes is only readily detectable in the absence of *Trf5*, the TRAMP5 RNA exosome can mask subtle transcriptional defects (Figure 4D). While we cannot rule out potential effects of *Fpr3* and *Fpr4* on the stability of RNAs, given the role histone chaperones play in nucleosome dynamics, we favor a model that explains this bias as a consequence of altered passage of polymerase through genes. Additional experiments probing transcriptional processivity in  $\Delta fpr3$  and

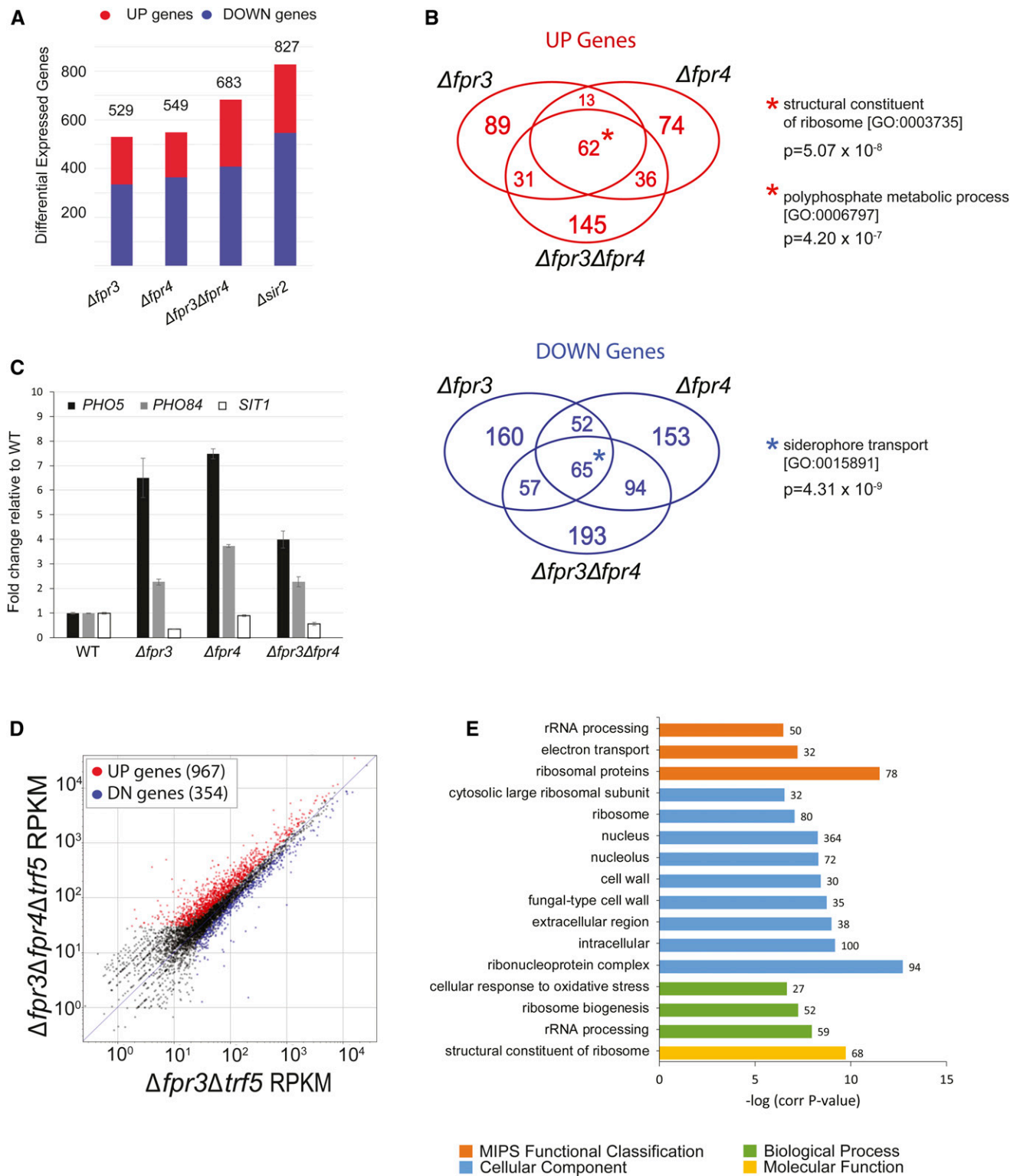


**Figure 4** *Fpr3* and *Fpr4* have partially overlapping effects on the transcriptome. (A) Numbers of differentially expressed genes in  $\Delta fpr3$ ,  $\Delta fpr4$ ,  $\Delta fpr3\Delta fpr4$ , and  $\Delta sir2$  mutants. (B) Venn diagrams depict the partial overlap in up- and downregulated genes in  $\Delta fpr3$ ,  $\Delta fpr4$ , and  $\Delta fpr3\Delta fpr4$  mutants. Genes at the centers of the diagrams (\*) are differentially expressed in all three RNA-seq data sets and are enriched in the indicated gene ontology terms. (C) Confirmation of select differentially expressed genes (*PHO5*, *PHO84*, and *SIT1*) by quantitative real-time PCR of RNA isolated from independent biological replicates. Fold changes in gene expression are shown relative to wild type. (D) Comparing the transcriptome of  $\Delta fpr3\Delta fpr4\Delta trf5$  triple deletion mutants to  $\Delta fpr3\Delta trf5$  double mutants reveals an increase number *Fpr4*-repressed RNAs (red dots). (E) Gene ontology enrichment analysis for upregulated transcripts in  $\Delta fpr3\Delta fpr4\Delta trf5$  triple deletion mutants. Enriched genes were classified by molecular function, biological process, cellular component, and Munich Information Center for Protein Sequences (MIPS) functional database classification by FunSpec (<http://funspec.med.utoronto.ca/>). WT, wild type.

$\Delta fpr4$  mutant yeast are needed to resolve the mechanism(s) by which these histone chaperones facilitate the full transcription of genes.

### ***Fpr4* inhibits transcription from the nontranscribed spacers of rDNA**

The rDNA locus in yeast consists of a series of 150–200 tandem repeats of a 9.1 kb unit containing the 35S and the 5S rRNAs, each separated by two nontranscribed spacer sequences (*NTS1* and *NTS2*) (Johnston *et al.* 1997). Given the nucleolar enrichment of *Fpr3* and *Fpr4*, and the ability of *Fpr4* to repress reporter expression from rDNA (Kuzuhara and Horikoshi 2004), we asked if yeast lacking *Fpr3* and *Fpr4* display transcriptional defects at rDNA. While our RNA-seq analysis was performed on ribo-minus RNA, reads from within the rRNA are readily detected (presumably from incomplete rRNA depletion) and indicate no change in rRNAs in  $\Delta fpr3$ ,  $\Delta fpr4$ , or  $\Delta fpr3\Delta fpr4$  strains (Figure 6A), which we have also observed in Northern and quantitative real-time PCR analyses (data not shown). Surprisingly, we did not observe evidence for the reported loss of *NTS* silencing in  $\Delta fpr4$  (or  $\Delta fpr3$  or  $\Delta fpr3\Delta fpr4$ ) yeast (Kuzuhara and Horikoshi 2004) (Figure 6A). Given that TRAMP5 buffers the loss of *Fpr4* (Figure 4D), we asked if *Trf5* might be degrading *NTS* RNAs in  $\Delta fpr4$  yeast. Consistent with this idea, we observe transcripts templated from both strands of *NTS1* and *NTS2* in  $\Delta fpr3\Delta fpr4\Delta trf5$ , but not  $\Delta fpr3\Delta trf5$  strains. Taken together, these results support a model where *Fpr4* establishes a transcriptionally silent chromatin state at rDNA. In the absence of this chromatin structure, pervasive transcription can occur from both strands of *NTS1* and *NTS2*. These RNAs are presumably normally degraded by TRAMP5.

### ***Fpr3* and *Fpr4* are required for genomic stability at rDNA**

Ribosomal RNAs comprise ~80% of the total RNA in yeast; accordingly, active rDNA repeats are the most heavily transcribed and nucleosome-free genes in the cell (Warner 1999; Vogelauer *et al.* 2000; Nomura *et al.* 2004). Reciprocally, the adjacent *NTS* spacers and inactive rDNA repeats are chromatinized and potentially silenced. This arrangement is thought to generate a chromatin template that is refractory to recombination between rDNA repeats and the deleterious loss of rDNAs from chromosome XII, which is a major driver of yeast replicative aging (Sinclair and Guarente 1997). For this reason, failure to generate heterochromatin environments at rDNA, as occurs in  $\Delta sir2$  histone deacetylase mutants, decreases genomic stability at this locus (Gottlieb and Esposito 1989; Kobayashi *et al.* 2004).

We reasoned that if *Fpr3* or *Fpr4* were silencing the *NTS* regions via a mechanism that involves chromatin structure, that yeast lacking these enzymes should also exhibit genomic instability at this locus. To test this hypothesis, we introduced  $\Delta fpr3\Delta fpr4$  and  $\Delta sir2$  deletions into a strain with a reporter gene (*URA3*) integrated at *NTS1* (van Leeuwen and Gottschling 2002; van Leeuwen *et al.* 2002). First, *URA*<sup>+</sup> status of each strain was ensured by propagation in media

lacking uracil. Next, cells were grown in nonselective media (YPD) for 2 days to permit reporter silencing or loss. Phenotypically *ura*<sup>-</sup> cells were isolated on 5-FOA and ~96 colonies were picked using a colony picking robot. These *ura*<sup>-</sup> cells could arise in two ways: epigenetic silencing of *URA3* at *NTS1*, or from *URA3* gene loss via recombination (Figure 7A). To discriminate between these events, we replica-plated these individual isolates to media lacking uracil, where growth indicates that the *URA3* phenotype was a consequence of epigenetic silencing. Reciprocally, isolates that failed to grow would represent reporter loss events (Figure 7A). These propagation assays revealed that normally, the rate of epigenetic switching of *URA3* is much higher than reporter loss: 82% of *ura*<sup>-</sup> isolates still have a *URA3* gene at the end of our propagation assay as exemplified growth in the absence of uracil (Figure 7, B and C), and by PCR of genomic DNA (not shown). As expected,  $\Delta sir2$  yeast are unable to establish silent chromatin at *NTS1*, and can only grow on 5-FOA via loss of the reporter. Finally, we observe that  $\Delta fpr3\Delta fpr4$  yeast are compromised in their ability to silence *URA3* epigenetically: only 30% of 5-FOA-resistant colonies retain the *URA3* gene. Thus, in  $\Delta fpr3\Delta fpr4$  yeast recombination and *URA3* reporter gene loss are more frequent than epigenetic silencing. This observation supports a model where *Fpr3* and *Fpr4* build chromatin structures at the *NTS* regions of rDNA locus. These structures are critical to maintaining genome stability at rDNA.

## **Discussion**

Gene duplication events play a critical role in protein and organism evolution. However, the high similarity of duplicated genes can lead to complete or partial compensation when one paralog is deleted, as is in the case in conventional genetic interaction analysis. Here we present a dual-query SGA screening approach where one genetic cross can report the separate, shared, and masked genetic interactions of gene paralogs. Using this approach on two nucleoplasm-like histone chaperones revealed that they perform separate, cooperative, and redundant chromatin-related functions. Given that ~13% of yeast protein coding genes are duplicates (Wolfe and Shields 1997), this approach may have applications in the analysis of other paralogs.

The genetic interactions annotated here support a unique function for *Fpr3* in orchestrating centromeric chromatin dynamics during chromosome segregation. This is fully consistent with existing literature (Hochwagen *et al.* 2005; Krogan *et al.* 2006; Macqueen and Roeder 2009; Ghosh and Cannon 2013; Ohkuni *et al.* 2014). Our comparative analysis provides additional systems-level evidence that this role is not shared with *Fpr4*, indicating that *Fpr3*, potentially as a homo-oligomer, may regulate chromatin in a way that affects chromosome segregation (Hochwagen *et al.* 2005; Macqueen and Roeder 2009). Furthermore, the fact that  $\Delta fpr3\Delta fpr4$  double mutants display fewer

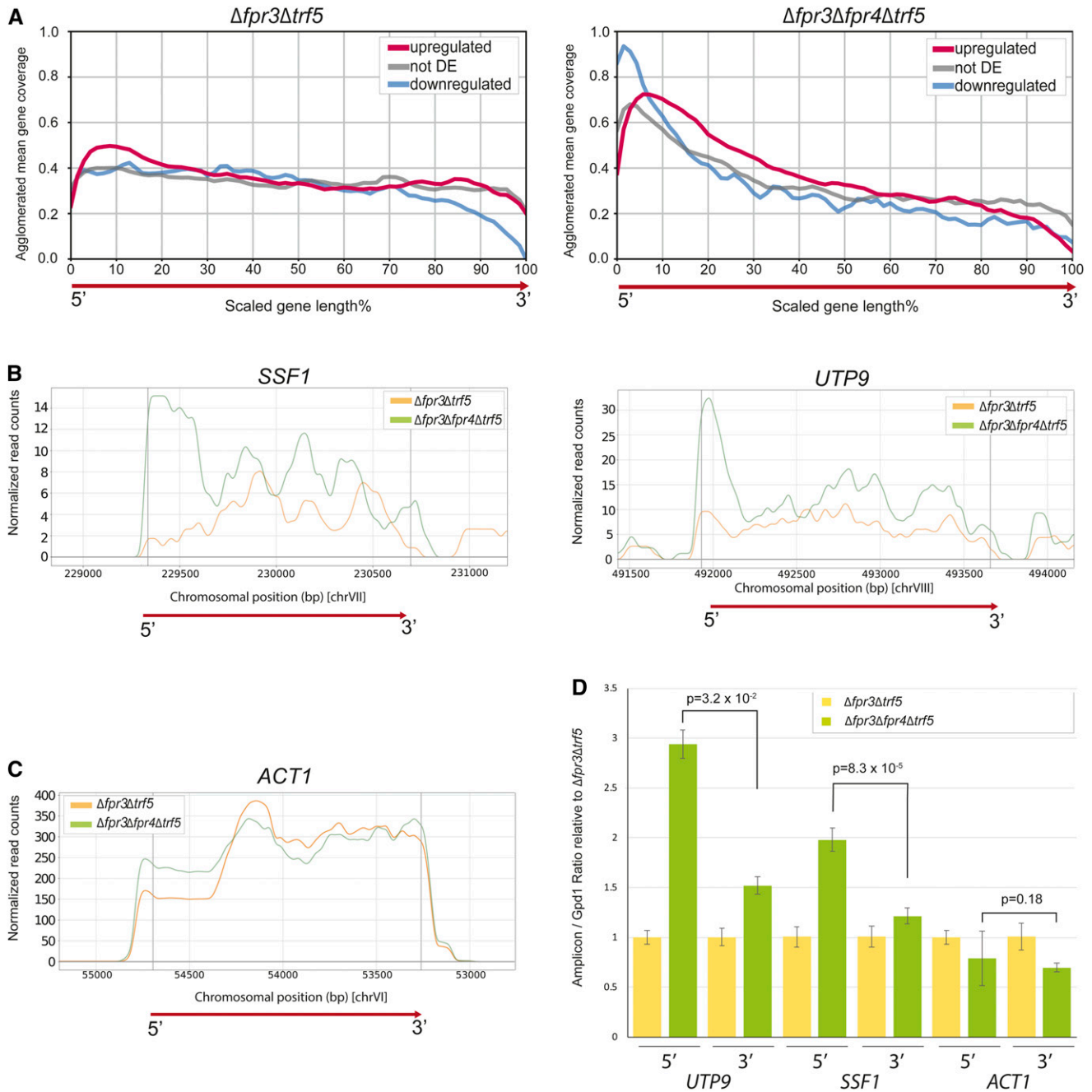


**Figure 5** A signature of incomplete elongation is present in  $\Delta fpr4$  yeast. (A) Plots of RNA-seq read density as a function of position on a scaled average gene. Upregulated, downregulated, and unchanged transcripts generated from (left)  $\Delta fpr3\Delta trf5$  double mutants and (right)  $\Delta fpr3\Delta fpr4\Delta trf5$  triple mutants are shown. (B) RNA-seq read density plots on two genes showing a signature of incomplete elongation: (left) *SSF1*, (right) *UTP9*. (C) RNA-seq read density plots on *ACT1*, a gene without a signature of incomplete elongation. (D) Quantitative real-time PCR validation of RNA read densities on *UTP9*, *SSF1*, and *ACT1*. 5' and 3' amplicons were normalized to the unchanged *GPD1* gene. RNAs were extracted from independent biological replicates (from those subjected to RNA-seq).

genetic interactions than single-gene  $\Delta fpr3$  mutants (Appendix 1) indicates that *Fpr4* may be toxic in the absence of *Fpr3* (Ohkuni *et al.* 2014). This model predicts that in the absence of *Fpr3*, the partial engagement or modification of chromatin by *Fpr4* is deleterious.

Several members of the ADA and SWI/SNF chromatin regulatory complexes exhibit negative genetic interactions

with both *Fpr3* and *Fpr4*. These results could be explained by reduced dosage of a histone chaperone activity. Alternately, these genetic interactions are consistent with a model where *Fpr3* and *Fpr4* act together to chaperone nucleosomes, facilitating chromatin dynamics as SWI/SNF does. Whether this means that the paralogs operate together in a sequence of events, such as the removal and subsequent redeposition

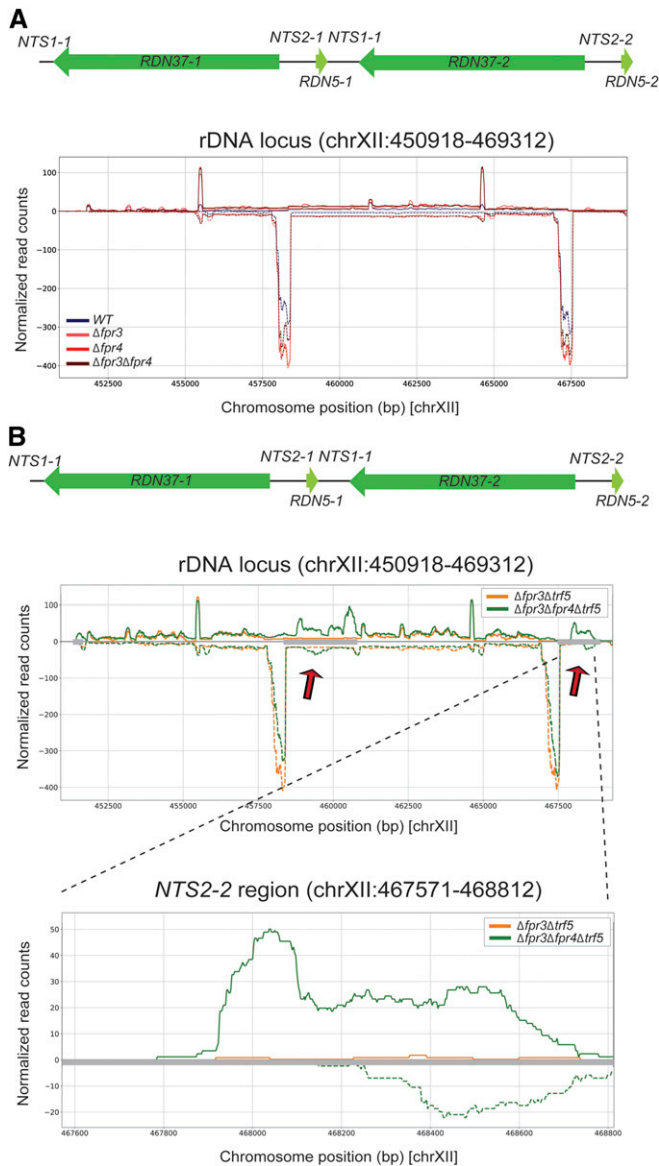


**Figure 6** *Fpr4* is required to silence the nontranscribed spacers (NTS) of rDNA. (A) Plots of RNA-seq read density across the rDNA locus on chromosome XII in wild type and  $\Delta fpr3$ ,  $\Delta fpr4$ , and  $\Delta fpr3\Delta fpr4$  mutants. The lack of reads mapping to NTS2-1, NTS1-1 (center) and NTS2-2 (right) suggests transcriptional silence is maintained in all strains. (B) Plots of RNA-seq read density across the rDNA locus on chromosome XII (top), and across NTS2-2 (bottom) in wild type and  $\Delta fpr3\Delta trf5$  and  $\Delta fpr3\Delta fpr4\Delta trf5$  mutants. The reads mapping to NTS2-1, NTS1-1 (center) and NTS2-2 (right) in  $\Delta fpr3\Delta fpr4\Delta trf5$  reveals that *Fpr4* is required to transcriptionally silence the NTSs. WT, wild type.

of nucleosomes during transcription or, in concert as a hetero-oligomeric complex, is not yet clear. The fact that *Fpr3* and *Fpr4* copurify (Krogan *et al.* 2006) supports the latter model, but does not exclude the former.

The repression of several phosphate and polyphosphate metabolism genes in rich media requires both *Fpr3* and *Fpr4*. It is therefore intriguing that both *Fpr3* and *Fpr4* were recently identified as two of the most heavily polyphosphorylated proteins in the yeast proteome, along with several

proteins in an evolutionarily conserved network of ribosome biogenesis factors (Neef and Klädde 2003; Bentley-DeSousa *et al.* 2018). The precise sites of *Fpr3* and *Fpr4* polyphosphorylation and the effect of this post-translational modification on *Fpr3* and *Fpr4* function is not yet clear. *Fpr3* and *Fpr4* also affect the steady-state levels of mRNAs encoding ribosomal protein genes and rRNA processing machinery. Thus, *Fpr3* and *Fpr4* may function as master regulators of ribosome biogenesis by coordinating both ribosomal protein abundance and rRNA processing. Given that many ribosomal and rRNA processing protein genes are driven by common regulators, *Fpr3* and *Fpr4* may recognize common DNA sequences or transcription factors to accomplish this function (Fermi *et al.* 2016). As already stated, the links between polyphosphorylation of *Fpr3* and *Fpr4* and the ribosome biogenesis network also require further investigation. It appears that at least some elements of this regulatory system may be conserved in the human nuclear FKBP25 protein (Gudavicius *et al.* 2014; Dilworth *et al.* 2017) and the acidic tract-containing nucleolin protein (Bentley-DeSousa *et al.* 2018).

The yeast TRAMP5 complex recognizes and polyadenylates aberrant RNA transcripts to target them for degradation by the *Rrp6* ribonuclease (Schmidt and Butler 2013). TRAMP5 targets include both ribosomal protein coding mRNAs and cryptic unstable transcripts generated from intragenic sites on the genome, including those within the rDNA locus (LaCava *et al.* 2005; Reis and Campbell 2007; San Paolo *et al.* 2009; Wery *et al.* 2009). Here, we found that deletion of  $\Delta trf5$  enabled the detection of a previously invisible transcriptome signature  $\Delta fpr4$  yeast where there is a bias in the RNA-seq reads toward the 5' end of genes. This is consistent with *Fpr4* promoting the transcriptional elongation process. It is noteworthy that these reads appear to cover the first one to three nucleosomes of genes because *Fpr4* is capable of both histone and nucleosome binding (Leung *et al.* 2017), and was previously shown to be important for the kinetics of transcriptional induction (Nelson *et al.* 2006). Thus, the nucleosomes near the transcriptional start site are candidates targets of *Fpr4*. This regulation could involve either the installation of nucleosomes within promoters to inhibit transcriptional initiation or nucleosome/histone eviction from sequences downstream of the promoter to remove nucleosome blocks to the polymerase. The cryo-electron microscopy structures of nucleoplasm pentamers engaging intact histone octamers provides further support for these models (Franco *et al.* 2019). We recently showed that *Fpr4*'s nucleoplasm-like acidic regions bind to free histones, while its basic surfaces permit nucleosome binding (Leung *et al.* 2017). Precisely how these activities and *Fpr4*'s peptidyl-prolyl isomerase activity toward the histone H3 tail (Nelson *et al.* 2006) (Monneau *et al.* 2013) cooperate to regulate chromatin dynamics is still unclear. However, the genetic and transcriptional readouts identified here provide complementary assays for dissecting the importance of each of these features.

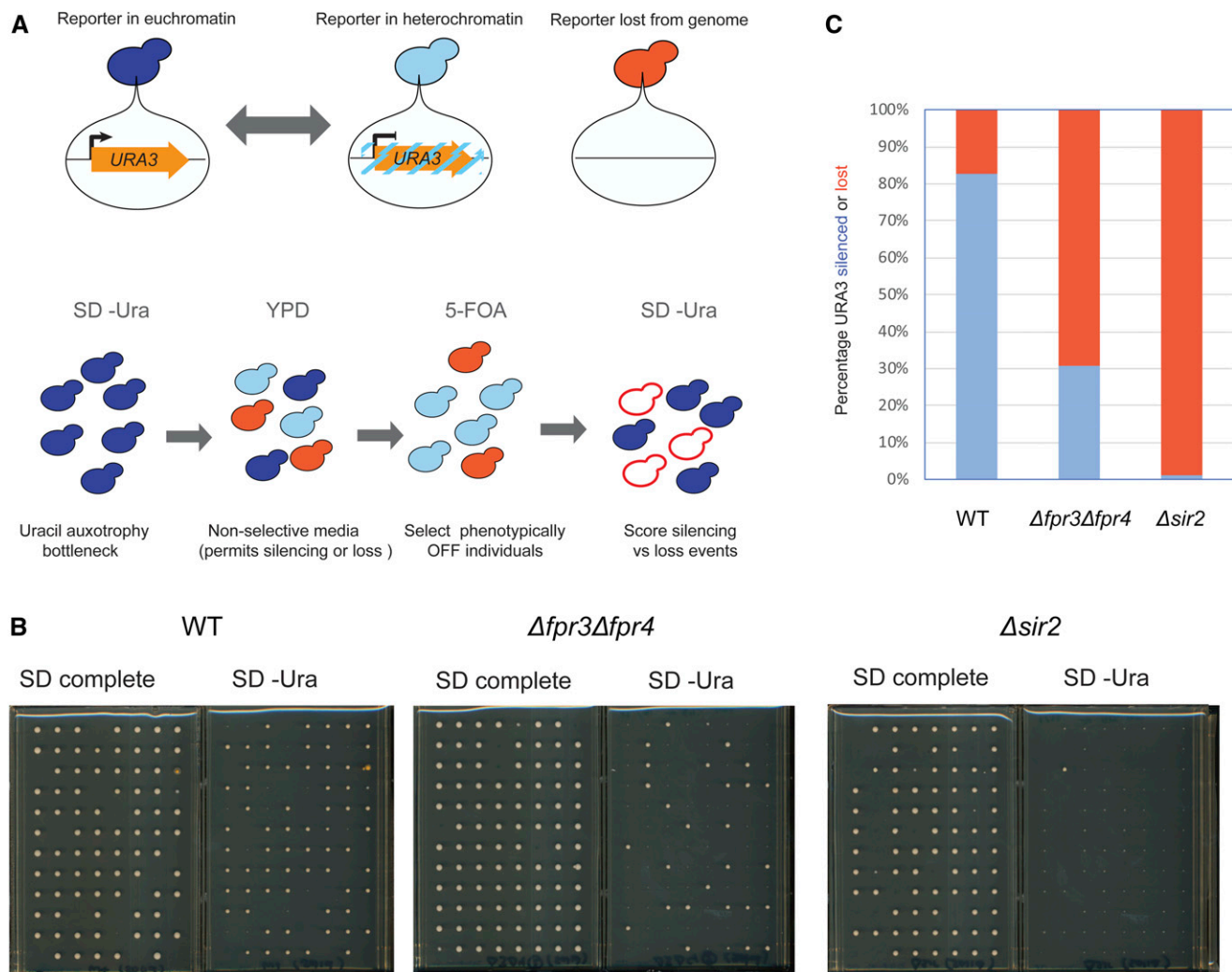


**Figure 7** *Fpr3* and *Fpr4* are required for genomic stability at the rDNA locus. (A) Diagrams illustrating the propagation experiment carried out to assess frequency of reporter loss. Top: the rDNA(NTS1)::*URA3* gene stochastically switches between an active euchromatin state (dark blue cells) and a silenced heterochromatin-like state (light blue cells). Bottom: individuals that lose the reporter due to instability can be distinguished from cells with a stochastically silenced reporter with the indicated workflow. (B) Images of the 96 individuals selected for after propagation on SD complete control media and SD-URA experimental media. Those growing on the experimental media represent the fraction of the population in which the reporter was epigenetically silenced. Those that fail to grow indicate permanent loss of the reporter. (C) Percentage of total colonies recovered after strain propagation that have retained or lost the ability to grow on SD complete media. WT, wild type.

In addition to regulating the transcription of protein coding genes, *Fpr4* restricts transcription from the NTS sequences of rDNA. This is consistent with both nucleolar enrichment and data indicating that *Fpr4* inhibits transcription of exogenous reporters at rDNA in yeast (Kuzuhara and Horikoshi 2004) and orthologs operate similarly in plants (Li and Luan 2010). In yeast, the NTS loci contain important DNA sequence features, including two terminators for the RNA Pol I-transcribed RDN35 repeat, a replication fork barrier site, and an autonomous replication site. Two separate observations suggest that *Fpr4* builds chromatin at rDNA to insulate DNA at these spacers. First, using a strain sensitized to reveal *Fpr4*-regulated RNAs accumulates large amounts of NTS transcripts, and these RNAs are templated by both DNA

strands. Second, consistent with a chromatin structural defect underpinning this phenomenon, the rDNA locus in  $\Delta fpr3\Delta fpr4$  yeast is also hyper-recombinogenic (Figure 7). Thus, these histone chaperones are of particular importance at the 100–200 rRNA repeats where they mediate the stability and silencing of spacers between the most heavily transcribed sequences in the cell. How these chaperones regulate chromatin structure at this locus, and how the structure differs from other targets in the nuclear genome, remain open questions that can now be addressed in future studies.

### Acknowledgments

The authors declare they have no conflict of interest.

## Literature Cited

- Basson, M. E., M. Thorsness, and J. Rine, 1986 *Saccharomyces cerevisiae* contains two functional genes encoding 3-hydroxy-3-methylglutaryl-coenzyme A reductase. *Proc. Natl. Acad. Sci. USA* 83: 5563–5567. <https://doi.org/10.1073/pnas.83.15.5563>
- Bentley-DeSousa, A., C. Holinier, H. Moteshareie, Y. C. Tseng, S. Kajjo *et al.*, 2018 A screen for candidate targets of lysine polyphosphorylation uncovers a conserved network implicated in ribosome biogenesis. *Cell Rep.* 22: 3427–3439. <https://doi.org/10.1016/j.celrep.2018.02.104>
- Benton, B. M., J. H. Zang, and J. Thorner, 1994 A novel FK506- and rapamycin-binding protein (FPR3 gene product) in the yeast *Saccharomyces cerevisiae* is a proline rotamase localized to the nucleolus. *J. Cell Biol.* 127: 623–639. <https://doi.org/10.1083/jcb.127.3.623>
- Bridges, C. B., 1936 The bar “gene” a duplication. *Science* 83: 210–211. <https://doi.org/10.1126/science.83.2148.210>
- Collins, S. R., K. M. Miller, N. L. Maas, A. Roguev, J. Fillingham *et al.*, 2007 Functional dissection of protein complexes involved in yeast chromosome biology using a genetic interaction map. *Nature* 446: 806–810. <https://doi.org/10.1038/nature05649>
- Costanzo, M., A. Baryshnikova, J. Bellay, Y. Kim, E. D. Spear *et al.*, 2010 The genetic landscape of a cell. *Science* 327: 425–431. <https://doi.org/10.1126/science.1180823>
- Costanzo M., B. VanderSluis, E. N. Koch, A. Baryshnikova, C. Pons, *et al.*, 2016 A global genetic interaction network maps a wiring diagram of cellular function. *Science* 353: aaf1420. <https://doi.org/10.1126/science.aaf1420>
- Darlington, C. D., and A. A. Moffett, 1930 Primary and secondary chromosome balance in *Pyrus*. *J. Genet.* 22: 129–151. <https://doi.org/10.1007/BF02983843>
- Davey, M., C. Hannam, C. Wong, and C. J. Brandl, 2000 The yeast peptidyl proline isomerases FPR3 and FPR4, in high copy numbers, suppress defects resulting from the absence of the E3 ubiquitin ligase TOM1. *Mol. Gen. Genet.* 263: 520–526. <https://doi.org/10.1007/s004380051197>
- Dilworth, D., S. K. Upadhyay, P. Bonnafous, A. B. Edo, S. Bourbigot *et al.*, 2017 The basic tilted helix bundle domain of the prolyl isomerase FKBP25 is a novel double-stranded RNA binding module. *Nucleic Acids Res.* 45: 11989–12004. <https://doi.org/10.1093/nar/gkx852>
- Dolinski, K., S. Muir, M. Cardenas, and J. Heitman, 1997 All cyclophilins and FK506 binding proteins are, individually and collectively, dispensable for viability in *Saccharomyces cerevisiae*. *Proc. Natl. Acad. Sci. USA* 94: 13093–13098. <https://doi.org/10.1073/pnas.94.24.13093>
- Dutta, S., I. V. Akey, C. Dingwall, K. L. Hartman, T. Laue *et al.*, 2001 The crystal structure of nucleoplasmic core: implications for histone binding and nucleosome assembly. *Mol. Cell* 8: 841–853. [https://doi.org/10.1016/S1097-2765\(01\)00354-9](https://doi.org/10.1016/S1097-2765(01)00354-9)
- Edlich-Muth, C., J. B. Artero, P. Callow, M. R. Przewloka, A. A. Watson *et al.*, 2015 The pentameric nucleoplasmic fold is present in *Drosophila* FKBP39 and a large number of chromatin-related proteins. *J. Mol. Biol.* 427: 1949–1963. <https://doi.org/10.1016/j.jmb.2015.03.010>
- Ellahi, A., D. M. Thurtle, and J. Rine, 2015 The chromatin and transcriptional landscape of native *saccharomyces cerevisiae* telomeres and subtelomeric domains. *Genetics* 200: 505–521. <https://doi.org/10.1534/genetics.115.175711>
- Fermi, B., M. C. Bosio, and G. Dieci, 2016 Promoter architecture and transcriptional regulation of Abf1-dependent ribosomal protein genes in *Saccharomyces cerevisiae*. *Nucleic Acids Res.* 44: 6113–6126. <https://doi.org/10.1093/nar/gkw194>
- Force, A., M. Lynch, F. B. Pickett, A. Amores, Y. L. Yan *et al.*, 1999 Preservation of duplicate genes by complementary, degenerative mutations. *Genetics* 151: 1531–1545. <https://doi.org/10.1016/j.gde.2010.11.175>
- Francino, M. P., 2005 An adaptive radiation model for the origin of new gene functions. *Nat. Genet.* 37: 573–577. <https://doi.org/10.1038/ng1579>
- Franco, A., R. Arranz, N. Fernández-Rivero, A. Velázquez-Campoy, J. Martín-Benito *et al.*, 2019 Structural insights into the ability of nucleoplasmic core to assemble and chaperone histone octamers for DNA deposition. *Sci. Rep.* 9: 9487. <https://doi.org/10.1038/s41598-019-45726-7>
- Ghosh, A., and J. F. Cannon, 2013 Analysis of protein phosphatase-1 and aurora protein kinase suppressors reveals new aspects of regulatory protein function in *Saccharomyces cerevisiae*. *PLoS One* 8: e69133. <https://doi.org/10.1371/journal.pone.0069133>
- Gottlieb, S., and R. E. Esposito, 1989 A new role for a yeast transcriptional silencer gene, SIR2, in regulation of recombination in ribosomal DNA. *Cell* 56: 771–776. [https://doi.org/10.1016/0092-8674\(89\)90681-8](https://doi.org/10.1016/0092-8674(89)90681-8)
- Gudavicius, G., D. Dilworth, J. J. Serpa, N. Sessler, E. V. Petrotchenko *et al.*, 2014 The prolyl isomerase, FKBP25, interacts with RNA-engaged nucleolin and the pre-60S ribosomal subunit. *RNA* 20: 1014–1022. <https://doi.org/10.1261/rna.042648.113>
- Hochwagen, A., W.-H. H. Tham, G. A. Brar, and A. Amon, 2005 The FK506 binding protein Fpr3 counteracts protein phosphatase 1 to maintain meiotic recombination checkpoint activity. *Cell* 122: 861–873. <https://doi.org/10.1016/j.cell.2005.07.010>
- Houseley, J., and D. Tollervey, 2008 The nuclear RNA surveillance machinery: the link between ncRNAs and genome structure in budding yeast? *Biochim. Biophys. Acta. Gene Regul. Mech.* 1779: 239–246. <https://doi.org/10.1016/j.bbagr.2007.12.008>
- Hughes, A. L., 1994 The evolution of functionally novel proteins after gene duplication. *Proc. Biol. Sci.* 256: 119–124. <https://doi.org/10.1098/rspb.1994.0058>
- Huh, W.-K., J. V. Falvo, L. C. Gerke, A. S. Carroll, R. W. Howson *et al.*, 2003 Global analysis of protein localization in budding yeast. *Nature* 425: 686–691. <https://doi.org/10.1038/nature02026>
- Innan, H., and F. Kondrashov, 2010 The evolution of gene duplications: classifying and distinguishing between models. *Nat. Rev. Genet.* 11: 97–108. <https://doi.org/10.1038/nrg2689>
- Johnston, M., L. Hillier, L. Riles, K. Albermann, B. André *et al.*, 1997 The nucleotide sequence of *Saccharomyces cerevisiae* chromosome XII. *Nature* 387: 87–90. <https://doi.org/10.1038/387s087>
- Kataoka, T., S. Powers, C. McGill, O. Fasano, J. Strathern *et al.*, 1984 Genetic analysis of yeast RAS1 and RAS2 genes. *Cell* 37: 437–445. [https://doi.org/10.1016/0092-8674\(84\)90374-X](https://doi.org/10.1016/0092-8674(84)90374-X)
- Kellis, M., B. W. Birren, and E. S. Lander, 2004 Proof and evolutionary analysis of ancient genome duplication in the yeast *Saccharomyces cerevisiae*. *Nature* 428: 617–624. <https://doi.org/10.1038/nature02424>
- Kobayashi, T., T. Horiuchi, P. Tongaonkar, L. Vu, and M. Nomura, 2004 SIR2 regulates recombination between different rDNA repeats, but not recombination within individual rDNA genes in yeast. *Cell* 117: 441–453. [https://doi.org/10.1016/S0092-8674\(04\)00414-3](https://doi.org/10.1016/S0092-8674(04)00414-3)
- Koztowska, M., A. Tarczewska, M. Jakób, D. Bystranowska, M. Taube *et al.*, 2017 Nucleoplasmic-like domain of FKBP39 from *Drosophila melanogaster* forms a tetramer with partly disordered tentacle-like C-terminal segments. *Sci. Rep.* 7: 1–14. <https://doi.org/10.1038/srep40405>
- Krogan, N. J., G. Cagney, H. Yu, G. Zhong, X. Guo *et al.*, 2006 Global landscape of protein complexes in the yeast *Saccharomyces cerevisiae*. *Nature* 440: 637–643. <https://doi.org/10.1038/nature04670>
- Kuzuhara, T., and M. Horikoshi, 2004 A nuclear FK506-binding protein is a histone chaperone regulating rDNA silencing. *Nat. Struct. Mol. Biol.* 11: 275–283. <https://doi.org/10.1038/nsmb733>

- LaCava, J., J. Houseley, C. Saveanu, E. Petfalski, E. Thompson *et al.*, 2005 RNA degradation by the exosome is promoted by a nuclear polyadenylation complex. *Cell* 121: 713–724. <https://doi.org/10.1016/j.cell.2005.04.029>
- Leung, A., F.-P. Jardim, N. Savic, Y. R. Monneau, R. González-Romero *et al.*, 2017 Basic surface features of nuclear FKBP5 facilitate chromatin binding. *Sci. Rep.* 7: 3795. <https://doi.org/10.1038/s41598-017-04194-7>
- Li, H., and R. Durbin, 2010 Fast and accurate short-read alignment with Burrows-Wheeler transform. *Bioinformatics* 26: 589–595. <https://doi.org/10.1093/bioinformatics/btp698>
- Li, H., and S. Luan, 2010 AtFKBP53 is a histone chaperone required for repression of ribosomal RNA gene expression in Arabidopsis. *Cell Res.* 20: 357–366. <https://doi.org/10.1038/cr.2010.22>
- Li, M., V. Valsakumar, K. Poorey, S. Bekiranov, and J. S. Smith, 2013 Genome-wide analysis of functional sirtuin chromatin targets in yeast. *Genome Biol.* 14: R48. <https://doi.org/10.1186/gb-2013-14-5-r48>
- Macqueen, A. J., and G. S. Roeder, 2009 Fpr3 and Zip3 ensure that initiation of meiotic recombination precedes chromosome synapsis in budding yeast. *Curr. Biol.* 19: 1519–1526. <https://doi.org/10.1016/j.cub.2009.08.048>
- Manning-Krieg, U. C., R. Henríquez, F. Cammas, P. Graff, S. Gavériaux *et al.*, 1994 Purification of FKBP-70, a novel immunophilin from *Saccharomyces cerevisiae*, and cloning of its structural gene, FPR3. *FEBS Lett.* 352: 98–103. [https://doi.org/10.1016/0014-5793\(94\)00927-9](https://doi.org/10.1016/0014-5793(94)00927-9)
- Milliman, E. J., N. Yadav, Y. C. Chen, B. Muddukrishna, S. Karunanithi *et al.*, 2012 Recruitment of Rpd3 to the telomere depends on the protein arginine methyltransferase Hmt1. *PLoS One* 7: e44656 [corrigenda: *PLoS One* 10: e0120968 (2015)]. <https://doi.org/10.1371/journal.pone.0044656>
- Monneau, Y. R., H. Soufari, C. J. Nelson, and C. D. Mackereth, 2013 Structure and activity of the peptidyl-prolyl isomerase domain from the histone chaperone Fpr4 toward histone H3 proline isomerization. *J. Biol. Chem.* 288: 25826–25837. <https://doi.org/10.1074/jbc.M113.479964>
- Neef, D. W., and M. P. Kladde, 2003 Polyphosphate loss promotes SNF/SWI- and gcn5-dependent mitotic induction of PHO5. *Mol. Cell Biol.* 23: 3788–3797. <https://doi.org/10.1128/MCB.23.11.3788-3797.2003>
- Nelson, C. J., H. Santos-Rosa, and T. Kouzarides, 2006 Proline isomerization of histone H3 regulates lysine methylation and gene expression. *Cell* 126: 905–916. <https://doi.org/10.1016/j.cell.2006.07.026>
- Nomura M., Y. Nogi, and M. Oakes, 2004 *Transcription of rDNA in the Yeast Saccharomyces cerevisiae*, Landes Bioscience, Austin TX.
- Ohkuni, K., R. Abdulle, and K. Kitagawa, 2014 Degradation of centromeric histone H3 variant Cse4 requires the Fpr3 peptidyl-prolyl cis-trans isomerase. *Genetics* 196: 1041–1045. <https://doi.org/10.1534/genetics.114.161224>
- Ohno, S., 1970 Part 3: why gene duplication? pp. 59–88 in *Evolution by Gene Duplication*, Springer-Verlag, Berlin, Germany.
- Park, S.-K., H. Xiao, and M. Lei, 2014 Nuclear FKBP5, Fpr3 and Fpr4 affect genome-wide genes transcription. *Mol. Genet. Genomics* 289: 125–136. <https://doi.org/10.1007/s00438-013-0794-0>
- Pemberton, T. J., 2006 Identification and comparative analysis of sixteen fungal peptidyl-prolyl cis/trans isomerase repertoires. *BMC Genomics* 7: 244. <https://doi.org/10.1186/1471-2164-7-244>
- Reis, C. C., and J. L. Campbell, 2007 Contribution of Trf4/5 and the nuclear exosome to genome stability through regulation of histone mRNA levels in *Saccharomyces cerevisiae*. *Genetics* 175: 993–1010. <https://doi.org/10.1534/genetics.106.065987>
- San Paolo, S., S. Vanacova, L. Schenk, T. Scherrer, D. Blank *et al.*, 2009 Distinct roles of non-canonical poly(A) polymerases in RNA metabolism. *PLoS Genet.* 5: 13–17. <https://doi.org/10.1371/journal.pgen.1000555>
- Schmidt, K. I., and J. S. Butler, 2013 Nuclear RNA surveillance: role of TRAMP in controlling exosome specificity. *Wiley Interdiscip Rev* 4: 217–231. <https://doi.org/10.1002/wrna.1155>
- Schmitt, M. E., T. A. Brown, and B. L. Trumppower, 1990 A rapid and simple method for preparation of RNA from *Saccharomyces cerevisiae*. *Nucleic Acids Res.* 18: 3091–3092. <https://doi.org/10.1093/nar/18.10.3091>
- Shan, X., Z. Xue, and T. Mélése, 1994 Yeast NPI46 encodes a novel prolyl cis-trans isomerase that is located in the nucleolus. *J. Cell Biol.* 126: 853–862. <https://doi.org/10.1083/jcb.126.4.853>
- Sinclair, D. A., and L. Guarente, 1997 Extrachromosomal rDNA circles—a cause of aging in yeast. *Cell* 91: 1033–1042. [https://doi.org/10.1016/S0092-8674\(00\)80493-6](https://doi.org/10.1016/S0092-8674(00)80493-6)
- Stirling, P. C., M. S. Bloom, T. Solanki-Patil, S. Smith, P. Sipahimalani *et al.*, 2011 The complete spectrum of yeast chromosome instability genes identifies candidate cancer genes and functional roles for astral complex components. *PLoS Genet.* 7: e1002057. <https://doi.org/10.1371/journal.pgen.1002057>
- Sydorsky, Y., D. J. Dilworth, B. Halloran, E. C. Yi, T. Makhnevych *et al.*, 2005 Nop53p is a novel nucleolar 60 S ribosomal subunit biogenesis protein. *Biochem. J.* 388: 819–826. <https://doi.org/10.1042/BJ20041297>
- Tarasov, A., A. J. Vilella, E. Cuppen, I. J. Nijman, and P. Prins, 2015 Sambamba: fast processing of NGS alignment formats. *Bioinformatics* 31: 2032–2034. <https://doi.org/10.1093/bioinformatics/btv098>
- Tong, A. H. Y., and C. Boone, 2006 Synthetic genetic array analysis in *Saccharomyces cerevisiae*. *Methods Mol. Biol.* 313: 171–192.
- Utsugi, T., A. Hirata, Y. Sekiguchi, T. Sasaki, A. Toh-e *et al.*, 1999 Yeast tom1 mutant exhibits pleiotropic defects in nuclear division, maintenance of nuclear structure and nucleocytoplasmic transport at high temperatures. *Gene* 234: 285–295. [https://doi.org/10.1016/S0378-1119\(99\)00197-3](https://doi.org/10.1016/S0378-1119(99)00197-3)
- van Leeuwen, F., P. R. Gafken, and D. E. Gottschling, 2002 Dot1p modulates silencing in yeast by methylation of the nucleosome core. *Cell* 109: 745–756. <https://doi.org/10.1016/S0092-867400759-6>
- van Leeuwen, F., and D. E. Gottschling, 2002 Assays for gene silencing in yeast. *Methods Enzymol.* 350: 165–186. [https://doi.org/10.1016/S0076-6879\(02\)50962-9](https://doi.org/10.1016/S0076-6879(02)50962-9)
- Vogelauer, M., F. Cioci, L. Bordin, G. Camilloni, B. Molecolare *et al.*, 2000 In vivo studies of the non-transcribed spacer region of rDNA in *Saccharomyces cerevisiae*. *Food Technol. Biotechnol.* 38: 315–321.
- Warner, J. R., 1999 The economics of ribosome biosynthesis in yeast. *Trends Biochem. Sci.* 24: 437–440. [https://doi.org/10.1016/S0968-0004\(99\)01460-7](https://doi.org/10.1016/S0968-0004(99)01460-7)
- Wery, M., S. Ruidant, S. Schillewaert, N. Leporé, and D. L. J. Lafontaine, 2009 The nuclear poly(A) polymerase and Exosome cofactor Trf5 is recruited cotranscriptionally to nucleolar surveillance. *RNA* 15: 406–419. <https://doi.org/10.1261/rna.1402709>
- Wolfe, K. H., and D. C. Shields, 1997 Molecular evidence for an ancient duplication of the entire yeast genome. *Nature* 387: 708–713. <https://doi.org/10.1038/42711>
- Wolin, S. L., S. Sim, and X. Chen, 2012 Nuclear noncoding RNA surveillance: is the end in sight? *Trends Genet.* 28: 306–313. <https://doi.org/10.1016/j.tig.2012.03.005>
- Xiao, H., V. Jackson, and M. Lei, 2006 The FK506-binding protein, Fpr4, is an acidic histone chaperone. *FEBS Lett.* 580: 4357–4364. <https://doi.org/10.1016/j.febslet.2006.06.093>
- Young, B. P., and C. J. R. Loewen, 2013 Balony: a software package for analysis of data generated by synthetic genetic array experiments. *BMC Bioinformatics* 14: 354. <https://doi.org/10.1186/1471-2105-14-354>

Communicating editor: O. Rando